

---

# CLIP-GS: CLIP-INFORMED GAUSSIAN SPLATTING FOR REAL-TIME AND VIEW-CONSISTENT 3D SEMANTIC UNDERSTANDING

---

**Guibiao Liao**  
Peking University

**Jiankun Li**  
Baidu Inc.

**Zhenyu Bao**  
Peking University

**Xiaoqing Ye**  
Baidu Inc.

**Jingdong Wang**  
Baidu Inc.

**Qing Li**  
Peng Cheng Laboratory

**Kanglin Liu**  
Peng Cheng Laboratory

## ABSTRACT

The recent 3D Gaussian Splatting (GS) exhibits high-quality and real-time synthesis of novel views in 3D scenes. Currently, it primarily focuses on geometry and appearance modeling, while lacking the semantic understanding of scenes. To bridge this gap, we present CLIP-GS, which integrates semantics from Contrastive Language-Image Pre-Training (CLIP) into Gaussian Splatting to efficiently comprehend 3D environments without annotated semantic data. In specific, rather than straightforwardly learning and rendering high-dimensional semantic features of 3D Gaussians, which significantly diminishes the efficiency, we propose a Semantic Attribute Compactness (SAC) approach. SAC exploits the inherent unified semantics within objects to learn compact yet effective semantic representations of 3D Gaussians, enabling highly efficient rendering (>100 FPS). Additionally, to address the semantic ambiguity, caused by utilizing view-inconsistent 2D CLIP semantics to supervise Gaussians, we introduce a 3D Coherent Self-training (3DCS) strategy, resorting to the multi-view consistency originated from the 3D model. 3DCS imposes cross-view semantic consistency constraints by leveraging refined, self-predicted pseudo-labels derived from the trained 3D Gaussian model, thereby enhancing precise and view-consistent segmentation results. Extensive experiments demonstrate that our method remarkably outperforms existing state-of-the-art approaches, achieving improvements of 17.29% and 20.81% in mIoU metric on Replica and ScanNet datasets, respectively, while maintaining real-time rendering speed. Furthermore, our approach exhibits superior performance even with sparse input data, verifying the robustness of our method.

**Keywords** 3D Gaussian Splatting · Real-time · View-consistent · 3D Scene Semantic Understanding · 3D Scene Reconstruction · Sparse-view

## 1 Introduction

Neural Radiance Fields (NeRFs) [1] and 3D Gaussian Splatting (3DGS) [2] have emerged as promising methods for achieving high-quality 3D scene representation from multi-view images. Existing methods have made remarkable advancements in rendering novel views that encompass both geometric and appearance details [1, 3, 4, 5, 6, 7, 8]. However, achieving a comprehensive semantic understanding of 3D scenes [9, 10, 11, 12, 13, 14, 15, 16, 17] remains a challenging task. To address this, one intuitive approach involves using manually annotated multi-view semantic labels to offer semantic supervision for existing 3D scene representations. Nevertheless, this resource-intensive process of manual annotation impedes its practical application in real-world 3D semantic understanding. Compared to the traditional semantic labeling manner, the 2D vision-language model Contrastive Language-Image Pre-Training (CLIP) is exploited to provide a new approach to semantic understanding without reliance on annotated image labels. The CLIP model comprises an image encoder and a text encoder, and undergoes pre-training on extensive image-text pairs sourced from websites to establish vision-language associations. This paradigm empowers the pre-trained CLIP model to exhibit

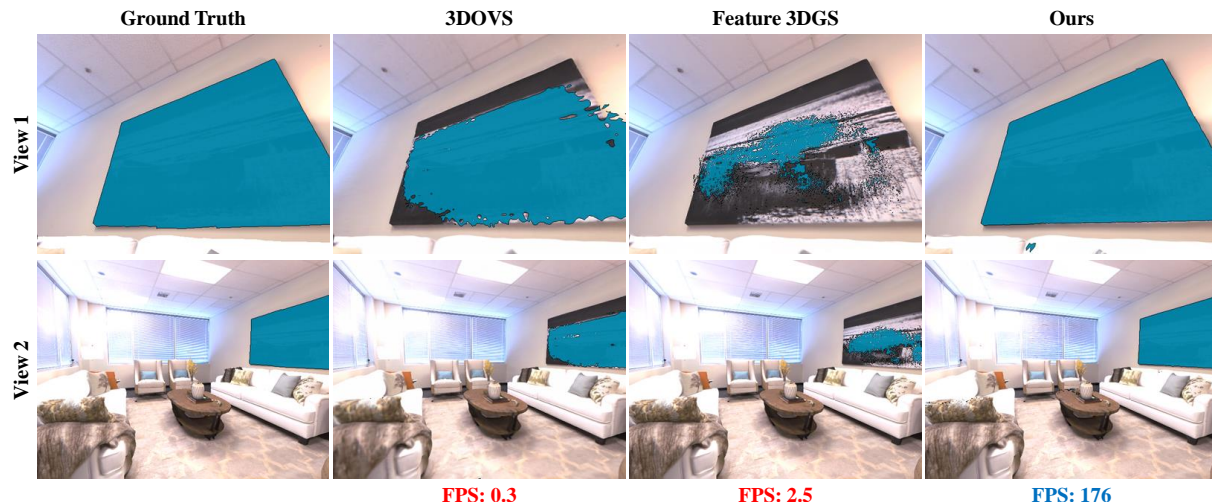


Figure 1: Visual comparisons between our approach and other CLIP-informed 3D semantic segmentation methods using the text query "Picture" across various views. *NeRF*-based approach 3DOVS [25] and *3DGS*-based method Feature 3DGS [26] exhibit ambiguous semantics and inefficiency, while our approach can achieve precise and consistent results alongside faster speed.

promising semantic understanding capabilities [18, 19, 20, 21, 22, 23, 24]. Consequently, how to effectively harness image-text knowledge from CLIP for precise 3D semantic understanding is emerging as a valuable and attractive area.

Recent endeavors [27, 25] have attempted to distill multi-view semantic features from the pre-trained CLIP model into *NeRF* for 3D semantic understanding. Concretely, LERF [27] constructs a semantic field based on *NeRF* and optimizes it by incorporating multi-view semantic features from the CLIP image encoder, allowing it to generate 3D segmentation results using textual descriptions. Similarly, 3DOVS [25] employs CLIP features to supervise the *NeRF*-based semantic field, and introduces a relevancy alignment loss to enhance the learning of the semantic field. However, *NeRF*'s ray-marching volume rendering technique imposes significant constraints on rendering efficiency, as depicted in the second column of Fig. 1.

To tackle this challenge, the up-to-date work, Feature 3DGS [26], exploits an alternative 3D representation, namely, 3D Gaussians [2], and employs tile-based rasterization for more efficient rendering. Specifically, Feature 3DGS follows 3DGS [2] that models the 3D scene through a set of 3D Gaussians. Additionally, for semantic modeling, Feature 3DGS embeds high-dimensional learnable semantic parameters into 3D Gaussians. These Gaussians, enriched with embedded semantics, are supervised using CLIP semantic features obtained from multiple training views.

However, certain limitations hinder its effectiveness in achieving efficient and precise 3D semantic understanding. **1) Efficiency Bottleneck.** Despite adopting a more efficient differentiable rasterization technique, Feature 3DGS still falls short of meeting the real-time (>30 FPS) requirement, as exhibited in the third column of Fig. 1. The primary factor contributing to this challenge is the high-dimensional semantic embeddings utilized in Feature 3DGS, which considerably decrease the efficiency of differentiable rasterization, consequently leading to an inefficient rendering result. **2) Deficient 3D Semantic Consistency.** When dealing with various views, the 2D CLIP model struggles to maintain consistent object identities. Thus, directly applying view-inconsistent semantics to optimize 3D Gaussians presents a challenge in obtaining consistent semantics across different views as illustrated in Fig. 1. Hence, efficiently modeling semantics with 3D Gaussians and effectively enhancing view-consistent semantic learning, pose challenges for 3D semantic understanding.

In this work, we present **CLIP-GS**, an efficient method for achieving precise label-free 3D semantic understanding using the 3D Gaussian representation. **To address the efficiency challenge**, we propose the Semantic Attribute Compactness (SAC) approach. The insight of SAC is leveraging the naturally unified semantic within objects to streamline representation, which is achieved by capturing the single representative semantic feature for each object using the masks from the Segment Anything Model (SAM) [28]. This process reduces redundant computations across similar features while preserving effective features. Additionally, we employ low-dimensional semantic index embeddings associated with 3D Gaussians during rasterization, leading to a more efficient semantic representation of 3D scenes (>100 FPS). **To address deficient 3D consistency**, we derive inspiration from the inherent consistent multi-view outputs of 3D models, and introduce 3D Coherent Self-training (3DCS). In 3DCS, self-predicted pseudo-labels are

produced from trained 3D Gaussians and then refined through the integration of cross-view semantics, facilitated by the SAM’s masks. This approach yields a view-consistent supervision signal, bolstering semantic consistency, as depicted in the last column of Fig. 1.

In summary, the main contributions of this work are as follows.

- We introduce a Semantic Attribute Compactness approach that efficiently represents compact and effective semantics using 3D Gaussians, ensuring extremely efficient rendering.
- We propose a 3D Coherent Self-training approach that addresses semantic ambiguity and forces consistency of coherent semantic representations across different views.
- Extensive experiments demonstrate that our approach outperforms state-of-the-art CLIP-informed 3D semantic understanding methods in both segmentation precision and rendering efficiency (>100 FPS). Moreover, our method shows superior performance in the sparse-view setting, validating its robustness.

## 2 Related Work

### 2.1 Gaussian Splatting for 3D Representation

Representing 3D scenes via radiance fields has witnessed significant advancements in recent years. For example, Neural Radiance Field (NeRF) [1, 8], utilizing a coordinate-based neural network, implicitly represents the appearance and geometry of 3D scenes. Despite substantial efforts to improve optimization and rendering efficiency [6, 5], NeRF-based methods continue to face challenges related to slow rendering speeds, primarily attributed to the query process of the neural network and volume rendering technique.

Recently, Kerbl et al. [2] proposed to represent a 3D scene as a collection of 3D Gaussians and leveraged a fast tile-based rasterizer technique, enabling real-time rendering at 1080p resolution with high-quality visual results. Building upon the efficiency demonstrated by 3D Gaussian Splatting in novel view synthesis, several studies have extended its application to various tasks. For instance, DreamGaussian [29] introduced a generative 3D Gaussian Splatting model with the designed mesh extraction and UV-space texture refinement algorithms to facilitate efficient text-to-3D content creation. Additionally, Wu et al. [30] proposed an explicit representation method for dynamic scenes, integrating both 3D Gaussians and 4D neural voxels. They devised a decomposed neural voxel encoding algorithm to construct Gaussian features, followed by the utilization of a lightweight MLP to predict Gaussian deformations at new timestamps. Meanwhile, [31] introduced the pioneering application of 3D Gaussian Splatting to incremental 3D reconstruction using a single moving monocular or RGB-D camera. This approach not only yielded impressive results in trajectory estimation but also enabled the reconstruction of minute and even transparent objects. Unlike these methods, our paper primarily focuses on harnessing 3D Gaussian Splatting for achieving 3D semantic understanding.

### 2.2 CLIP-Informed 3D Semantic Field

To build the 3D semantic field, some early methods attempt to distill CLIP features [32, 33] into NeRFs. DFF [34] explored the integration of feature vectors from CLIP-LSeg [18] to optimize the semantic feature field. LERF [27] extended the concept of feature alignment from CLIP to a scale-conditioned feature field, supervised through multi-scale CLIP features obtained from the CLIP image encoder. Similarly, 3DOVS [25] optimized the semantic feature field using CLIP features and introduced a relevance-distribution alignment loss to enhance semantic learning. However, these NeRF-based methods are hindered by the bottleneck of NeRF’s volume rendering, leading to challenges in achieving efficient rendering results.

Alternative to NeRFs, recent works explore embedding CLIP features into 3D Gaussian to construct a semantic field and employ a differentiable tile rasterizer technique for efficient semantic rendering. FMGS [35] integrated 3D Gaussians with multi-resolution hash encodings (MHE) to form a combined feature field, which was supervised by multi-view features obtained from CLIP models. Feature 3DGS [26] attached high-dimensional CLIP embeddings at 3D Gaussians, optimizing them using CLIP semantic features from multiple training views. However, embedding high-dimensional parameters at millions of 3D Gaussians in a scene significantly hampers training and rendering efficiency. Shi et al. [36] embedded quantized CLIP features onto massive 3D Gaussians for scene representation, aiming to reduce memory and storage demands. LangSplat [37] learned low-dimensional language features at 3D Gaussians and utilized a pre-trained deep convolutional neural network (CNN) network for upsampling rendered language features to align with CLIP features. Yet, pre-training the deep CNN network and employing a post-processing upsampling process inevitably introduce training and inference time, respectively.

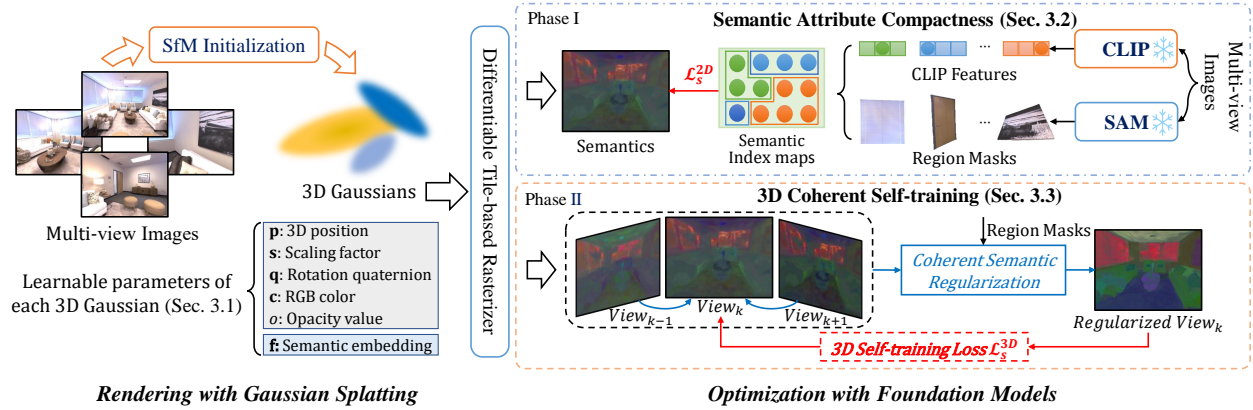


Figure 2: Illustration of CLIP-GS optimization. *Left*: A collection of 3D Gaussians with learnable attributes is initialized to represent the 3D scene following 3DGS [2], specifically with an additional attribute: the *semantic embedding*. Subsequently, these 3D Gaussian attributes are rendered into the 2D plane for optimization using a differentiable rasterizer. *Right*: First, multi-view images undergo feature extraction using the frozen CLIP model [32] and region mask generation using SAM [28]. Then, we optimize the CLIP-GS in an end-to-end manner, consisting of two phases. In Phase I, we introduce *Semantic Attribute Compactness (SAC)* to learn compact semantic representations of 3D Gaussians, facilitating highly efficient rendering. In Phase II, after training CLIP-GS a few times, we introduce *3D Coherent Self-training (3DCS)*. 3DCS leverages cross-view self-predicted semantics derived from CLIP-GS, enhanced by coherent regularization, to strengthen view-consistent supervision for Gaussians. The adaptive density control part and color optimization process are omitted for simplicity, as the same in 3DGS [2].

Unlike previous methods, our method addresses these limitations by introducing the semantic attribute compactness. This method efficiently represents the scene semantics with Gaussians, ensuring exceptionally swift training and inference speed. Additionally, we enhance 3D segmentation accuracy by proposing a 3D coherent self-training approach, which improves the view consistency of semantics for achieving precise 3D semantic understanding.

### 3 Methodology

Our approach endeavors to efficiently construct a comprehensive 3D scene representation that not only captures detailed appearance and geometry but also provides a precise semantic understanding of the 3D scene. To achieve this goal, we draw inspiration from recent advances in 3D Gaussian Splatting (3DGS) [2] and formulate our method, which exploits 3DGS from pure 3D reconstruction to encompass the semantic perception of 3D scenes. In this section, we first briefly present the preliminaries of 3D Gaussian Splatting (Sec. 3.1). Then, as shown in Fig. 2, we introduce a Semantic Attribute Compactness (SAC) approach that models efficient semantic representation based on Gaussians (Sec. 3.2). Moreover, we propose the 3D Coherent Self-training (3DCS) to improve 3D semantic consistency with a view-consistent semantic constraint strategy (Sec. 3.3). Finally, we present the overall training process (Sec. 3.4).

#### 3.1 Preliminaries of 3D Gaussian Splatting

3D Gaussian Splatting (3DGS) [2] represents a 3D scene using a suite of 3D Gaussians. The properties of each Gaussian include a 3D position  $\mathbf{p} = \{x, y, z\} \in \mathbb{R}^3$ , a 3D size scaling factor  $\mathbf{s} \in \mathbb{R}^3$ , a rotation quaternion  $\mathbf{q} \in \mathbb{R}^4$ , a color  $\mathbf{c} \in \mathbb{R}^3$ , and an opacity value  $o_i \in \mathbb{R}$ . These parameters are learnable and can be collectively symbolized by  $\Gamma_{\theta_i} = \{\mathbf{p}_i, \mathbf{s}_i, \mathbf{q}_i, \mathbf{c}_i, o_i\}$ , where  $i$  denotes the  $i$ -th Gaussian. Specifically, for computing the pixel color  $C$ , it utilizes  $\alpha$ -blending point-based rendering by blending  $\mathcal{N}$  points in the front-to-back depth order [38]:

$$C = \sum_{i \in \mathcal{N}} T_i \alpha_i \mathbf{c}_i, \quad (1)$$

where  $\mathcal{N}$  is the set of Gaussian points that overlap with the given pixel.  $\alpha_i$  is calculated by  $\alpha_i = o_i G_i^{2D}$ , where  $G_i^{2D}$  denotes the function of the  $i$ -th Gaussian projected onto 2D plane. The transmittance  $T_i$  is calculated as the product of opacity values of preceding Gaussians that overlap the same pixel:  $T_i = \prod_{j=1}^{i-1} (1 - \alpha_j)$ . The initial 3D Gaussians are constructed from the sparse data points created by Structure-from-Motion (SfM) [39] using COLMAP [40]. To

optimize these 3D Gaussians, Gaussian Splatting employs a differentiable rendering technique for projecting them onto the 2D image plane [41] and utilizes gradient-based color supervision to update parameters. The reconstruction loss is computed by minimizing the rendered image  $\hat{I}$  and the ground truth image  $I$  color, which is formulated as:

$$\mathcal{L}_{rgb} = (1 - \lambda)\mathcal{L}_1(\hat{I}, I) + \lambda\mathcal{L}_{D-SSIM}(\hat{I}, I), \quad (2)$$

where  $\lambda$  is set to 0.2. 3DGS has proven effective in 3D reconstruction tasks, showing more efficient inference speeds with high-quality reconstruction comparable to NeRF. However, its potential for 3D scene understanding remains unexplored. Our research showcases the considerable potential of 3D Gaussians in facilitating a comprehensive understanding of complex 3D scenes.

### 3.2 Semantic Attribute Compactness

To achieve semantic outputs via Gaussian splatting, an intuitive method is attaching a learnable semantic parameter  $\mathbf{f}_i \in \mathbb{R}^D$  at each Gaussian, and utilizing the above  $\alpha$ -blending rendering to compute the rendered pixel semantic  $F$ :

$$F = \sum_{i \in \mathcal{N}} T_i \alpha_i \mathbf{f}_i \in \mathbb{R}^D, \quad (3)$$

where  $D$  denotes the dimension of rendered semantic features and is typically set to a high-dimensional number, e.g., 512, to align the CLIP semantic feature dimension for optimizing  $\mathbf{f}_i$ . However, this direct embedding of high-dimensional parameters into a million Gaussians to modeling semantics greatly decreases the efficiency of the rasterization process, such as [26].

To tackle this efficiency challenge, we introduce the Semantic Attribute Compactness (SAC). The insight of SAC lies in leveraging the inherently unified semantic meaning of the identical object for efficient representation. Concretely, we represent each object by learning a representative semantic feature, minimizing the learning of redundant similar features within the object. Furthermore, we employ low-dimensional semantic index embeddings to represent these high-dimensional semantic features. These low-dimensional embeddings are attached to 3D Gaussians for rasterization, resulting in a more compact and efficient representation of scene semantics.

Specifically, for the input training view  $I_k$ , we transform the semantic features  $\tilde{S}_k \in \mathbb{R}^{D \times H \times W}$  obtained from CLIP into a representative version  $\hat{S}_k \in \mathbb{R}^{D \times M}$ , where  $M$  denotes the number of representative CLIP features in  $I_k$  and is much smaller than the image size  $H \times W$ . To achieve this, we harness the powerful Segment Anything Model (SAM) [28] to yield region masks  $R_k = \{R_k^q\}_{q=1}^M$  over the image  $I_k$ . Subsequently, for each region, we calculate the weighted average of the CLIP feature in the spatial dimension, which is treated as the unified feature to represent the semantics of this region uniformly. Through this manner, we can obtain the representative CLIP feature  $\hat{S}_k \in \mathbb{R}^{D \times M}$ . Furthermore, since the features are consistent for each region, we can leverage a semantic index for each region to represent the unified feature, resulting in the semantic index map  $M_k \in \mathbb{R}^{1 \times H \times W}$ . Through the SAC, the CLIP semantic feature of the input training image can be compactly represented by the unified feature and the low-dimensional semantic index map, symbolized by  $\tilde{S} = \hat{S} \circ M$ .

For optimization, we can embed a low-dimensional semantic learnable parameter  $\mathbf{f}_i \in \mathbb{R}^d$  into each 3D Gaussian, and then employ  $\alpha$ -blending rendering to learn the semantic index, which can be used to retrieve the CLIP features. To further expedite this learning process, we compute the retrieval process offline before training, which is given by  $\tilde{S} = \mathop{\text{argmax}}(\cos((M \circ \hat{S}), T)) \in \mathbb{R}^{1 \times H \times W}$ . Here, the text feature  $T$  is calculated using the CLIP text encoder to encode a set of text descriptions of  $C$  classes. During the optimization of the semantic parameters of 3D Gaussians, we project the 3D Gaussians onto the 2D plane with rasterization, and leverage a trainable lightweight convolution layer  $\mathcal{C}$  to align the classes' dimension  $C$ , obtaining the rendered semantic map:  $S = \mathcal{C}(\sum_{H,W} \sum_{i \in \mathcal{N}} T_i \alpha_i \mathbf{f}_i) \in \mathbb{R}^{C \times H \times W}$ . Then, the semantic loss of Gaussians is computed by:

$$\mathcal{L}_s^{2D} = \mathcal{L}_{ce}(S, \tilde{S}), \quad (4)$$

where  $\tilde{S}$  indicates the semantic representation of the training image derived from the proposed SAC offline. By enhancing 3D Gaussians with compact semantic representations, our method can construct 3D scene semantics efficiently, achieving extremely efficient rendering while maintaining high-quality visual results.

### 3.3 3D Coherent Self-training

Having achieved efficient semantic representations through semantic attribute compactness, however, immutably employing view-inconsistent CLIP semantics to optimize Gaussians leads to ambiguous and subpar rendering results, as shown in (a) of Fig. 3. This limitation stems from the inherent challenge of the 2D CLIP model in maintaining



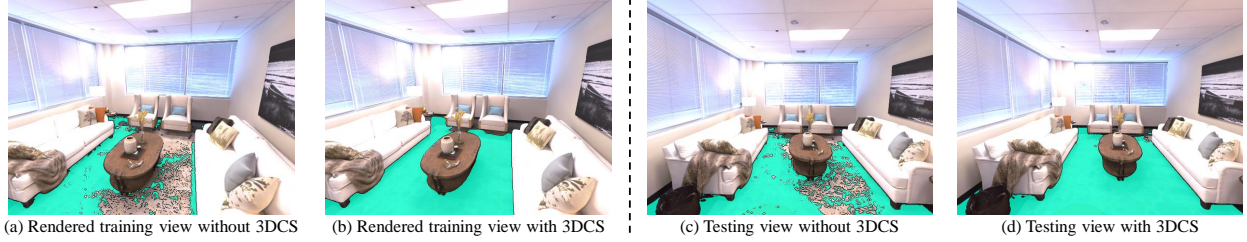


Figure 3: Illustration of rendered semantic maps with the text query "Rug". (a) and (b) correspond to training views, while (c) and (d) pertain to testing views. In (a), the rendered result appears ambiguous when immutably employing 2D CLIP semantics for Gaussian optimization. Conversely, (b) shows that leveraging 3DCS can provide coherent semantic constraints to supervise Gaussians, leading to more precise results (d). For more details refer to Sec. 3.3.

consistent object identities across various views, inadequately enforcing multi-view semantic consistency constraints. Inspired by the inherent 3D consistency of 3D models, we propose a 3D Coherent Self-training approach that utilizes view-consistent pseudo-labels from trained 3D Gaussians, imposing cross-view coherent semantic constraints for Gaussian optimization.

Specifically, after training 3D Gaussians a few times, the semantic map  $S_k$  at training view  $I_k$  is rendered from the 3D Gaussian representation. Then, we introduce a *coherent semantic regularization* by incorporating semantics of adjacent views to eliminate semantic ambiguity within the same object. To implement this, we treat the multi-view training images of the 3D scene as a sequence of continuous frames, akin to a video, and capitalize on the powerful zero-shot tracker [42] to associate the SAM’s masks across adjacent views. Next, semantic maps  $S_{k-1}$  and  $S_{k+1}$  are produced by rendering the 3D Gaussians to obtain the semantics of the preceding and subsequent views. For the  $q$ -th region  $R_k^q$  in the current view, we integrate semantic information from adjacent views  $R_{k-1}^q, R_{k+1}^q$  and enforce a coherent semantic regularization for region  $R_k^q$  to unify  $S_k^q$ . This regularization is accomplished through a majority voting mechanism, as formulated:  $S_k^q = \mathop{\text{argmax}}_c \sum_{v \in R_k^q} \mathbb{1}\{\mathop{\text{argmax}}(\sigma(\mathcal{C}(S_k^{qv}))) = c\}$ . Here,  $c$  indicates the  $c$ -th class and  $\mathbb{1}\{\cdot\}$  denotes the indicator function.  $\sigma$  denotes the softmax function. Similarly, all regions in the rendered semantic map  $S_k$  undergo regularization. As a result, it can be observed that the *rug* area of the current view exhibits consistent semantics, as illustrated in (b) of Fig. 3. Hence, we employ the more consistent supervision signal  $\mathcal{S}$  to train 3D Gaussians instead of using vanilla 2D CLIP semantics:

$$\mathcal{L}_s^{3D} = \mathcal{L}_{ce}(\mathcal{S}, \mathcal{S}). \quad (5)$$

Moreover, in each iteration, the 3D coherent self-training process only regularizes one training view, allowing for efficient training. Meanwhile, with more consistent constraints, 3D Gaussians are enhanced to exhibit more consistent semantics, in turn improving the more consistent semantic constraints in the next training epoch. As a result, this self-training pattern can facilitate view-consistent segmentation results, as demonstrated in the experiments.

### 3.4 Overall Training

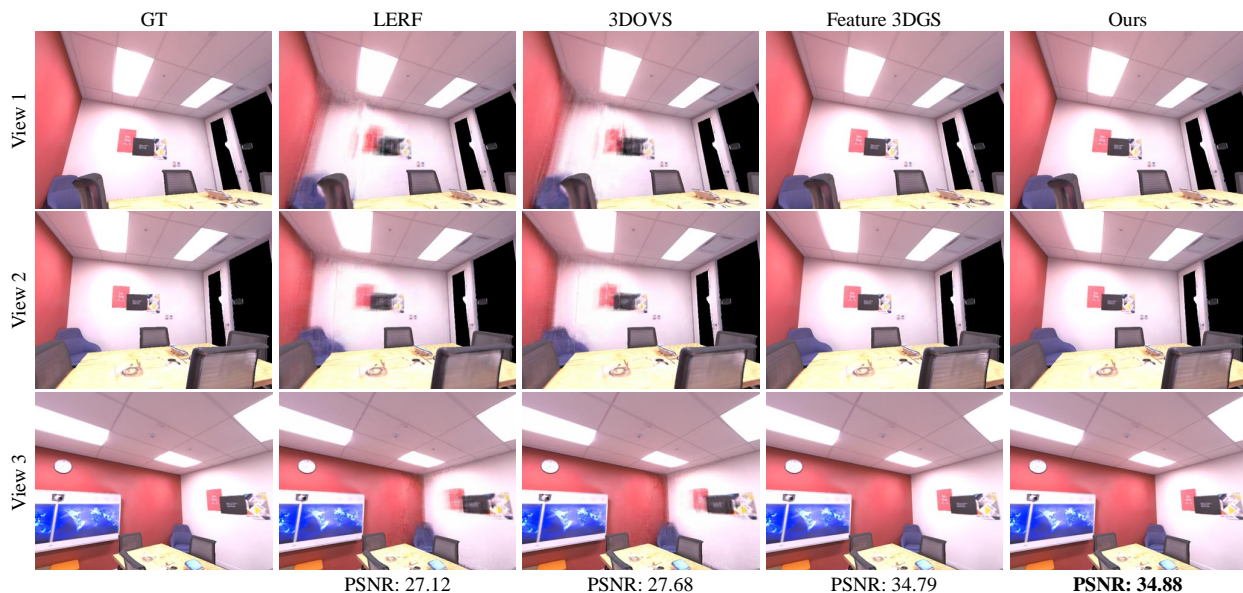
The entire model is trained end-to-end based on reconstruction loss  $\mathcal{L}_{rgb}$  and semantic loss  $\mathcal{L}_s$ , including two phases. In phase I, the semantic embeddings of 3D Gaussians are optimized using the semantic attribute compactness method based on  $\mathcal{L}_s^{2D}$ . In phase II, after training the 3D Gaussians a few iterations  $\mathcal{T}$ , the 3D self-training loss  $\mathcal{L}_s^{3D}$  is performed to replace the  $\mathcal{L}_s^{2D}$  for semantic consistency enhancement. This process can be formulated as:

$$\mathcal{L} = \begin{cases} \mathcal{L}_{rgb} + \mathcal{L}_s^{2D} & \text{Iteration} \leq \mathcal{T} \\ \mathcal{L}_{rgb} + \mathcal{L}_s^{3D} & \text{Iteration} > \mathcal{T}. \end{cases} \quad (6)$$

Furthermore, in 3DGS, loss computation initially spans the full image resolution, with Gaussian points densified every 100 iterations. This results in a proliferation of Gaussians, as their cloning or splitting using the density control strategy outlined in [2], impacting rasterization efficiency. To regulate the number of Gaussians for efficiency improvement while upholding high-quality scene representations, we introduce a Progressive Densification Regulation (PDR) strategy. With PDR, Gaussians are initially optimized at a lower image resolution with a reduced densification frequency. Subsequently, both the image resolution and densification frequency progressively increase over a period of training iterations until reaching the full resolution and default densification frequency. This approach prevents excessive focus on fine details to densify a large number of Gaussians at an early stage, while also slowing down the frequency of Gaussian increase. As exhibited in experiments, PDR effectively reduces the number of Gaussian points without compromising rendering quality, improving rendering efficiency.

Table 1: Quantitative comparison on reconstruction and segmentation results of novel views in Replica and ScanNet datasets, utilizing multi-view training data. Our approach achieves state-of-the-art performances with higher FPS efficiency.

Type	Method	FPS	Replica [43]					ScanNet [44]				
			PSNR	SSIM	LPIPS	mIoU	mAcc	PSNR	SSIM	LPIPS	mIoU	mAcc
<i>NeRF-based</i>	LERF [27]	0.2	31.034	0.904	0.103	8.285	22.125	24.921	0.778	0.392	15.349	40.294
	3DOVS [25]	0.3	31.373	0.908	0.091	9.081	23.938	24.915	0.780	0.389	17.802	42.532
<i>3DGS-based</i>	Feature 3DGS [26]	2.5	35.439	0.955	0.090	10.634	36.520	28.453	0.863	0.250	18.069	54.101
	Ours	176	35.481	0.955	0.090	27.919	67.776	29.057	0.866	0.250	38.876	79.465

Figure 4: Visual reconstruction results of novel view, using multi-view training data. Our method achieves photo-realistic rendering quality comparable to the Gaussian-based method, outperforming NeRF-based approaches.

## 4 Experiment

### 4.1 Experiment Setup

**Evaluation Datasets.** To evaluate the effectiveness of our approach, we conduct experiments on two widely-used multi-view indoor scene datasets: Replica [43] and ScanNet [44]. The Replica dataset consists of a series of high-quality indoor scenes, each with photo-realistic textures and per-primitive semantic classes. ScanNet contains a diverse set of real-world indoor scenes, each providing camera poses obtained from BundleFusion [45] and semantic segmentation labels. We experiment on six scenes from the Replica: Room0, Room1, Room2, Office0, Office2, and Office4, and four scenes from the ScanNet: scene0004, scene0389, scene0494, and scene0693. For each scene, 233 to 300 images are captured along a randomly chosen trajectory. Every tenth image is selected for evaluation, while the remaining images are used as training views.

Additionally, to evaluate the robustness of our method, we introduce a sparse-view benchmark. For each scene mentioned above, we evenly sample 30 images for the sparse view benchmark. Subsequently, we designate every tenth image as the testing image, with the remaining 27 images utilized for training data.

**Evaluation Metrics.** To evaluate the quality of reconstruction, we utilize three commonly used metrics: peak signal-to-noise (PSNR), the structural similarity index measure (SSIM), and the learned perceptual image patch similarity (LPIPS) [46]. Additionally, we report the mean Intersection-over-Union (mIoU) and mean pixel accuracy (mAcc) to measure the segmentation performance.

**Implementation Details.** We implement our approach based on PyTorch and Gaussian Splatting [2] on an NVIDIA A100 GPU. We follow the default parameter settings in Gaussian Splatting for scene reconstruction. To enable scene

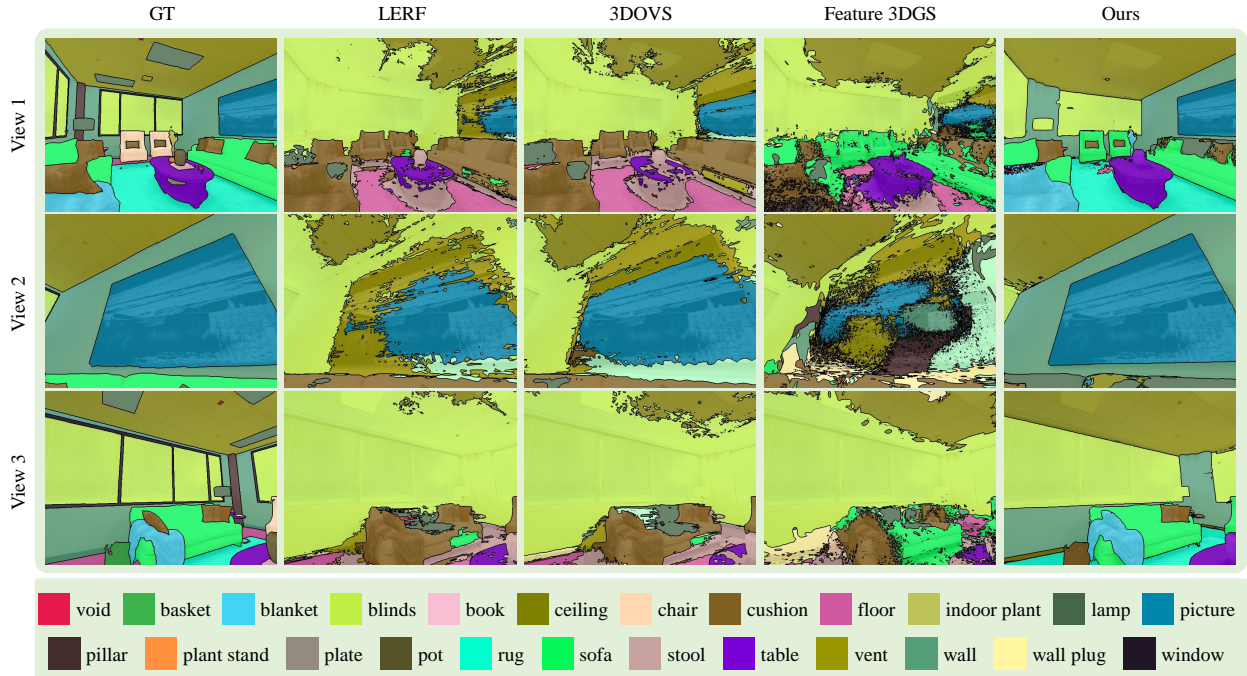


Figure 5: Visual segmentation results of novel view, using multi-view training data. Our method achieves more view-consistent and precise results across different views.

Table 2: Quantitative comparison on reconstruction and segmentation results of novel views, utilizing sparse-view training data. Our approach exhibits robust reconstruction quality and segmentation performance even with sparse input data.

Type	Method	Replica [43]					ScanNet [44]				
		PSNR	SSIM	LPIPS	mIoU	mAcc	PSNR	SSIM	LPIPS	mIoU	mAcc
<i>NeRF-based</i>	LERF [27]	17.509	0.697	0.484	4.312	17.080	20.819	0.719	0.429	14.059	38.734
	3DOVS [25]	17.923	0.708	0.477	4.553	19.356	21.414	0.723	0.422	14.227	40.584
<i>3DGS-based</i>	Feature 3DGS [26]	26.313	0.881	0.193	9.584	38.245	22.224	0.741	0.355	17.552	48.686
	Ours	26.366	0.881	0.196	24.300	67.329	22.736	0.754	0.347	37.965	73.678

understanding, we attach learnable semantic parameters of dimension  $d = 3$  to each 3D Gaussian. Additionally, we modify the CUDA kernel to ensure the semantic rasterization process while preserving the reconstruction quality. We utilize the CLIP ViT-B/16 model to extract image and text features, and employ the SAM ViT-H model to produce region masks. Before training, the CLIP features and SAM’s region masks of the training views are computed offline. During training, the learning rates for the semantic embedding and convolution layer are set to  $2.5e^{-3}$  and  $5e^{-4}$ , respectively. Adam optimizer is used to train our model for 30k iterations, with each scene taking about 20 minutes to train.  $\mathcal{T}$  is set to 15k to leverage the 3D coherent self-training method. For progressive densification regulation, we start by setting the training image resolution with a scale factor of 0.5 and the densification interval to 200 iterations. Then, we gradually increase the resolution to 1.0 and reduce the densification interval to 100 following a cosine scheme. The former occurs over the first 7k iterations and the latter in the initial 4k iterations.

## 4.2 Comparison with State-of-the-art Methods

We compare our approach both quantitatively and qualitatively with NeRF-based methods: LERF [27] and 3DOVS [25], and 3DGS-based method: Feature 3DGS [2]. Moreover, for a comprehensive evaluation, we introduce a sparse-view evaluation benchmark, a setup that trains the model solely using sparse training views.

**Quantitative Comparison.** We present the quantitative results in Table 1. We can observe that our method consistently outperforms other competitors in rendering quality and segmentation accuracy across diverse datasets. Notably, our





Figure 6: Visual reconstruction results of novel view, utilizing sparse-view training data. Our method exhibits less noise and finer details than competitors.

approach exhibits a significant improvement in mIoU of 17.285% and 20.807% over the second-best method on Replica and ScanNet, respectively. These results indicate a strong capability of our method to effectively leverage 3D Gaussians with compact and view-consistent semantic information, achieving precise 3D semantic understanding.

**Efficiency Comparison.** We report the frames per second (FPS) results to compare the inference speed of segmentation in Table 1. The evaluation is conducted at a  $640 \times 480$  image resolution using a single NVIDIA A100 GPU. We can see that NeRF-based methods exhibit slow inference speeds attributed to the volume rendering of NeRF. Despite using the splatting technique for accelerated rendering, Feature 3DGS encounters an efficiency bottleneck as it directly embeds high-dimensional semantic features into 3D Gaussians. In contrast, our approach efficiently attaches compact semantic information to 3D Gaussians by utilizing the proposed semantic attribute compactness, achieving a more efficient result.

**Qualitative Comparison.** Figures 4 and 5 display the qualitative results produced by our method alongside comparisons with other approaches, including reconstruction and segmentation. 1) In Fig. 4, we can observe that our method delivers better visual rendering quality across different views. 2) In Fig. 5, current SOTA methods present inaccurate and ambiguous segmentation results across diverse views. Differently, our approach exhibits spatially continuous and view-consistent semantics. These achievements can be attributed to our proposed 3D coherent self-training approach, which effectively leverages cross-view semantic coherent constraints, leading to more precise and 3D consistent results.

**Robustness Comparison.** We report the sparse-view quantitative comparisons in Table 2. Our approach, despite being trained using sparse views, consistently achieves superior performances in rendering quality and segmentation precision. Concretely, our method surpasses the second-best method by 14.716% and 20.413% in mIoU on Replica and ScanNet, respectively.

Besides, we provide visual comparisons in Fig. 6 and Fig. 7. We observe that 3DOVS is inclined to produce blurred visual results under sparse and unconstrained conditions, while Feature 3DGS exhibits coarse and ambiguous semantic results. In comparison, our method showcases more structural details and compact semantics in various scenes. These results can be attributed to our proposed 3D coherent self-training, which effectively integrates semantic information from adjacent views and enforces 3D consistency constraints, ensuing robustness even with sparse input data.

### 4.3 Ablation Studies

In Table 3, we conduct ablation studies to validate each component of our approach, including Semantic Attribute Compactness (SAC), 3D Coherent Self-training (3DCS), and Progressive Densification Regulation (PDR). Feature 3DGS [26] is employed as the baseline.

**Effect of SAC.** Compared to the baseline, SAC contributes to improvements in both inference efficiency and segmentation accuracy. This can be attributed to the SAC’s capacity to embed compact and effective semantic information into 3D Gaussians, facilitating efficient rendering and achieving precise segmentation results.

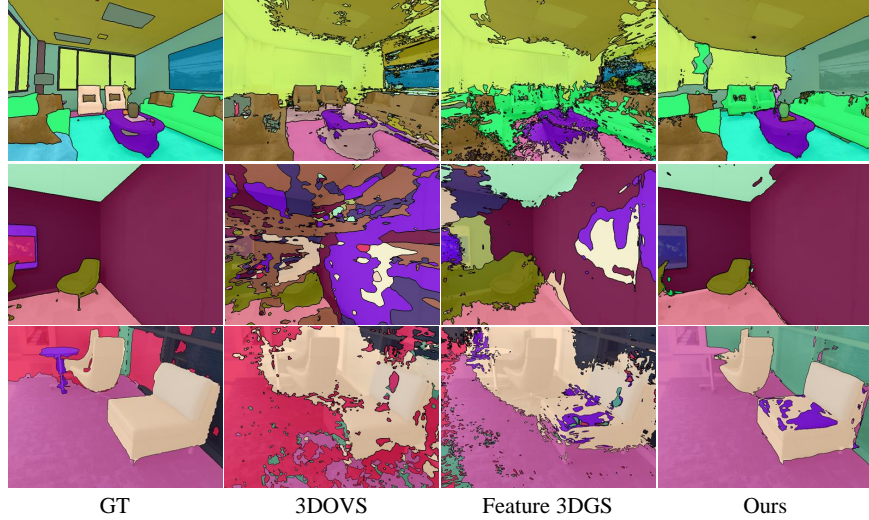


Figure 7: Visual segmentation results of novel view, utilizing sparse-view training data. Our approach obtains more robust and accurate segmentation performance.

Table 3: Ablation studies for our approach. The final configuration is denoted by Bold. More details refer to Sec. 4.3.

Index	Setting	FPS	Room0		Scene0494	
			mIoU	mAcc	mIoU	mAcc
(a)	Baseline	2.5	8.794	39.916	25.789	52.006
(b)	(a) + SAC	150	19.920	63.125	36.480	73.529
(c)	(b) + 3DCS	150	25.564	71.918	54.023	85.636
(d)	(c) + PDR (Ours)	176	<b>26.106</b>	<b>72.079</b>	<b>55.559</b>	<b>87.019</b>
(b1)	Ours ( $d=16$ )	150	26.694	71.568	55.862	86.792
(b2)	Ours ( $d=8$ )	166	26.134	71.422	55.397	87.026
(b3)	Ours ( $d=3$ )	176	<b>26.106</b>	<b>72.079</b>	<b>55.559</b>	<b>87.019</b>
(c1)	Ours ( $\mathcal{T}=10k$ )	176	25.524	70.930	53.847	85.133
(c2)	Ours ( $\mathcal{T}=15k$ )	176	<b>26.106</b>	<b>72.079</b>	<b>55.559</b>	<b>87.019</b>
(c3)	Ours ( $\mathcal{T}=20k$ )	176	25.235	71.472	53.225	84.722
(c4)	Ours ( $\mathcal{T}=25k$ )	176	23.552	70.748	51.676	82.918
(e)	Ours w/o coherent	176	24.654	71.551	37.538	75.352

**Effect of 3DCS.** As shown in (c), 3DCS achieves notable performance gains without adding extra computational overhead during inference. These results validate that 3DCS introduces essential view-consistent semantic constraints, mitigating ambiguous and coarse semantics and elevating the quality of coherent semantics.

**Effect of PDR.** As exhibited in (d), adding PDR boosts efficiency by reducing the number of Gaussians, e.g., from 1.72M to 1.43M in Room0. This indicates that PDR effectively constrains the optimization of 3D Gaussians.

**Effect of coherent in 3DCS.** In (e), "w/o coherent" denotes the absence of semantics from adjacent views for regularization. Instead, the semantics are only regularized using the current view's masks from SAM. The regularized semantics are then applied as  $\mathcal{S}$  in Equation 5. The decrease in performance verifies that incorporating semantics from adjacent views improves semantic consistency.

**Analysis of  $d$  in SAC.** We analyze the impact of different  $d$  in SAC, illustrated in (b1) - (b3). As  $d$  increases, the inference speed declines, coupled with a marginal improvement in mIoU. Therefore, we opt for  $d = 3$  as it delivers efficient yet competitive results.

**Analysis of  $\mathcal{T}$  in 3DCS.** We examine the influence of different settings of  $\mathcal{T}$ , as depicted in (c1) - (c4). Specifically,  $\mathcal{T} = 10k$  denotes the application of our 3D coherent self-training strategy after 10,000 training iterations. When  $\mathcal{T}$  is set to 15k, the model consistently achieves superior results, making it the chosen final configuration.

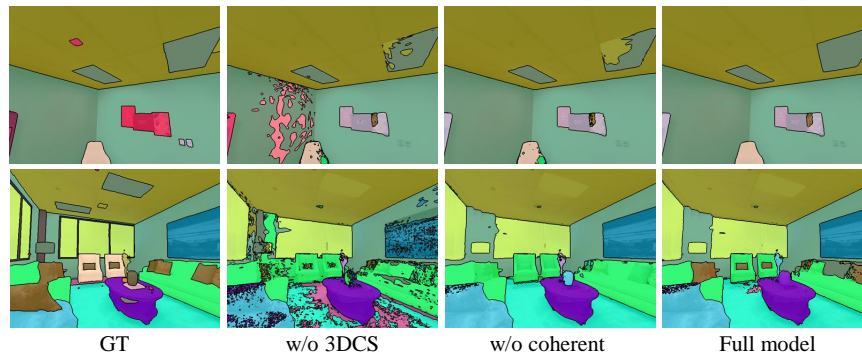


Figure 8: Visual comparison of ablation experiments.

Furthermore, we showcase visual ablation results in Fig. 8. Compared to the model without using 3DCS ("w/o 3DCS"), we can see that integrating 3D coherent self-training greatly reduces ambiguity and enhances semantic consistency, leading to spatially continuous results. Moreover, when compared to the model without introducing coherence ("w/o coherent"), incorporating semantics from adjacent views further enhances scene coherence. In summary, these qualitative results show the effectiveness of our proposed strategies for achieving precise 3D semantic understanding.

## 5 Conclusion

In this work, we present CLIP-GS, a novel approach utilizing Gaussian Splatting for achieving real-time and precise semantic understanding in 3D Scenes. Within CLIP-GS, the Semantic Attribute Compactness (SAC) attaches compact semantic information into 3D Gaussians to efficiently represent 3D semantics, ensuring highly efficient rendering. Furthermore, the proposed 3D Coherent Self-training (3DCS) enhances semantic consistency across different views, leading to accurate 3D segmentation results. Experimental results demonstrate that our approach significantly outperforms the SOTA methods on synthetic and real-world scenes. Besides, our method exhibits superior performance even with sparse input data, verifying the robustness of our 3D semantic learning approach.

## References

- [1] Ben Mildenhall, Pratul P Srinivasan, Matthew Tancik, Jonathan T Barron, Ravi Ramamoorthi, and Ren Ng. Nerf: Representing scenes as neural radiance fields for view synthesis. In *Proceedings of the European Conference on Computer Vision*, pages 405–421, 2020.
- [2] Bernhard Kerbl, Georgios Kopanas, Thomas Leimkühler, and George Drettakis. 3d gaussian splatting for real-time radiance field rendering. *ACM Transactions on Graphics*, 42(4), 2023.
- [3] Jonathan T Barron, Ben Mildenhall, Matthew Tancik, Peter Hedman, Ricardo Martin-Brualla, and Pratul P Srinivasan. Mip-nerf: A multiscale representation for anti-aliasing neural radiance fields. In *Proceedings of the IEEE/CVF International Conference on Computer Vision*, pages 5855–5864, 2021.
- [4] Jonathan T. Barron, Ben Mildenhall, Dor Verbin, Pratul P. Srinivasan, and Peter Hedman. Zip-nerf: Anti-aliased grid-based neural radiance fields. In *Proceedings of the IEEE/CVF International Conference on Computer Vision*, pages 19697–19705, 2023.
- [5] Anpei Chen, Zexiang Xu, Andreas Geiger, Jingyi Yu, and Hao Su. Tensorf: Tensorial radiance fields. In *Proceedings of the European Conference on Computer Vision*, pages 333–350, 2022.
- [6] Thomas Müller, Alex Evans, Christoph Schied, and Alexander Keller. Instant neural graphics primitives with a multiresolution hash encoding. *ACM Transactions on Graphics*, 41(4):1–15, 2022.
- [7] Zhenyu Bao, Guibiao Liao, Zhongyuan Zhao, Kanglin Liu, Qing Li, and Guoping Qiu. 3d reconstruction and new view synthesis of indoor environments based on a dual neural radiance field. *arXiv preprint arXiv:2401.14726*, 2024.
- [8] Kyle Gao, Yina Gao, Hongjie He, Dening Lu, Linlin Xu, and Jonathan Li. Nerf: Neural radiance field in 3d vision, a comprehensive review. *arXiv preprint arXiv:2210.00379*, 2022.

- [9] Chenguang Huang, Oier Mees, Andy Zeng, and Wolfram Burgard. Visual language maps for robot navigation. In *Proceedings of the IEEE International Conference on Robotics and Automation*, pages 10608–10615, 2023.
- [10] Xiaoyu Zhang, Guibiao Liao, Wei Gao, and Ge Li. Tdrnet: Transformer-based dual-branch restoration network for geometry based point cloud compression artifacts. In *2022 IEEE International Conference on Multimedia and Expo (ICME)*, pages 1–6. IEEE, 2022.
- [11] Di Feng, Christian Haase-Schütz, Lars Rosenbaum, Heinz Hertlein, Claudius Glaeser, Fabian Timm, Werner Wiesbeck, and Klaus Dietmayer. Deep multi-modal object detection and semantic segmentation for autonomous driving: Datasets, methods, and challenges. *IEEE Transactions on Intelligent Transportation Systems*, 22(3):1341–1360, 2020.
- [12] Krishna Murthy Jatavallabhula, Alihusein Kuwajerwala, Qiao Gu, Mohd Omama, Ganesh Iyer, Soroush Saryazdi, Tao Chen, Alaa Maalouf, Shuang Li, Nikhil Varma Keetha, Ayush Tewari, Joshua Tenenbaum, Celso de Melo, Madhava Krishna, Liam Paull, Florian Shkurti, and Antonio Torralba. Conceptfusion: Open-set multimodal 3d mapping. In *Proceedings of Robotics: Science and Systems*, 2023.
- [13] Guibiao Liao, Kaichen Zhou, Zhenyu Bao, Kanglin Liu, and Qing Li. Ov-nerf: Open-vocabulary neural radiance fields with vision and language foundation models for 3d semantic understanding. *arXiv preprint arXiv:2402.04648*, 2024.
- [14] Jiajun Deng, Wengang Zhou, Yanyong Zhang, and Houqiang Li. From multi-view to hollow-3d: Hallucinated hollow-3d r-cnn for 3d object detection. *IEEE Transactions on Circuits and Systems for Video Technology*, 31(12):4722–4734, 2021.
- [15] Guibiao Liao, Wei Gao, Qiuping Jiang, Ronggang Wang, and Ge Li. Mmnet: Multi-stage and multi-scale fusion network for rgb-d salient object detection. In *Proceedings of the ACM international conference on multimedia*, pages 2436–2444, 2020.
- [16] Wencan Huang, Daizong Liu, and Wei Hu. Dense object grounding in 3d scenes. In *Proceedings of the 31st ACM International Conference on Multimedia*, pages 5017–5026, 2023.
- [17] Yao Wu, Mingwei Xing, Yachao Zhang, Yuan Xie, Jianping Fan, Zhongchao Shi, and Yanyun Qu. Cross-modal unsupervised domain adaptation for 3d semantic segmentation via bidirectional fusion-then-distillation. In *Proceedings of the 31st ACM International Conference on Multimedia*, pages 490–498, 2023.
- [18] Boyi Li, Kilian Q Weinberger, Serge Belongie, Vladlen Koltun, and Rene Ranftl. Language-driven semantic segmentation. In *Proceedings of the International Conference on Learning Representations*, 2022.
- [19] Size Wu, Wenwei Zhang, Lumin Xu, Sheng Jin, Xiangtai Li, Wentao Liu, and Chen Change Loy. Clipself: Vision transformer distills itself for open-vocabulary dense prediction. In *Proceedings of the International Conference on Learning Representations*, 2024.
- [20] Ziyang Wang, Yunhao Gou, Jingjing Li, Lei Zhu, and Heng Tao Shen. Language-augmented pixel embedding for generalized zero-shot learning. *IEEE Transactions on Circuits and Systems for Video Technology*, 33(3):1019–1030, 2022.
- [21] Mengde Xu, Zheng Zhang, Fangyun Wei, Han Hu, and Xiang Bai. Side adapter network for open-vocabulary semantic segmentation. In *Proceedings of the IEEE/CVF Conference on Computer Vision and Pattern Recognition*, pages 2945–2954, 2023.
- [22] Guibiao Liao, Jiankun Li, and Xiaoqing Ye. Vlm2scene: Self-supervised image-text-lidar learning with foundation models for autonomous driving scene understanding. In *Proceedings of the AAAI Conference on Artificial Intelligence*, volume 38, pages 3351–3359, 2024.
- [23] Feng Liang, Bichen Wu, Xiaoliang Dai, Kunpeng Li, Yinan Zhao, Hang Zhang, Peizhao Zhang, Peter Vajda, and Diana Marculescu. Open-vocabulary semantic segmentation with mask-adapted clip. In *Proceedings of the IEEE/CVF Conference on Computer Vision and Pattern Recognition*, pages 7061–7070, 2023.
- [24] Hao Zhang, Feng Li, Xueyan Zou, Shilong Liu, Chunyuan Li, Jianwei Yang, and Lei Zhang. A simple framework for open-vocabulary segmentation and detection. In *Proceedings of the IEEE/CVF International Conference on Computer Vision*, pages 1020–1031, 2023.
- [25] Kunhao Liu, Fangneng Zhan, Jiahui Zhang, Muyu Xu, Yingchen Yu, Abdulmotaleb El Saddik, Christian Theobalt, Eric Xing, and Shijian Lu. Weakly supervised 3d open-vocabulary segmentation. In *Proceedings of the Advances in Neural Information Processing Systems*, 2023.
- [26] Shijie Zhou, Haoran Chang, Sicheng Jiang, Zhiwen Fan, Zehao Zhu, Dejia Xu, Pradyumna Chari, Suyu You, Zhangyang Wang, and Achuta Kadambi. Feature 3dgs: Supercharging 3d gaussian splatting to enable distilled feature fields. In *Proceedings of the IEEE/CVF Conference on Computer Vision and Pattern Recognition*, 2024.



- [27] Justin Kerr, Chung Min Kim, Ken Goldberg, Angjoo Kanazawa, and Matthew Tancik. Lerf: Language embedded radiance fields. In *Proceedings of the IEEE/CVF International Conference on Computer Vision*, pages 19729–19739, 2023.
- [28] Alexander Kirillov, Eric Mintun, Nikhila Ravi, Hanzi Mao, Chloe Rolland, Laura Gustafson, Tete Xiao, Spencer Whitehead, Alexander C. Berg, Wan-Yen Lo, Piotr Dollar, and Ross Girshick. Segment anything. In *Proceedings of the IEEE/CVF International Conference on Computer Vision*, pages 4015–4026, 2023.
- [29] Jiaxiang Tang, Jiawei Ren, Hang Zhou, Ziwei Liu, and Gang Zeng. Dreamgaussian: Generative gaussian splatting for efficient 3d content creation. In *Proceedings of the International Conference on Learning Representations*, 2024.
- [30] GuanJun Wu, Taoran Yi, Jiemin Fang, Lingxi Xie, Xiaopeng Zhang, Wei Wei, Wenyu Liu, Qi Tian, and Wang Xinggang. 4d gaussian splatting for real-time dynamic scene rendering. In *Proceedings of the IEEE/CVF Conference on Computer Vision and Pattern Recognition*, 2024.
- [31] Hidenobu Matsuki, Riku Murai, Paul H. J. Kelly, and Andrew J. Davison. Gaussian splatting slam. In *Proceedings of the IEEE/CVF Conference on Computer Vision and Pattern Recognition*, 2024.
- [32] Alec Radford, Jong Wook Kim, Chris Hallacy, Aditya Ramesh, Gabriel Goh, Sandhini Agarwal, Girish Sastry, Amanda Askell, Pamela Mishkin, Jack Clark, et al. Learning transferable visual models from natural language supervision. In *Proceedings of the International conference on machine learning*, pages 8748–8763. PMLR, 2021.
- [33] Mehdi Cherti, Romain Beaumont, Ross Wightman, Mitchell Wortsman, Gabriel Ilharco, Cade Gordon, Christoph Schuhmann, Ludwig Schmidt, and Jenia Jitsev. Reproducible scaling laws for contrastive language-image learning. In *Proceedings of the IEEE/CVF Conference on Computer Vision and Pattern Recognition*, pages 2818–2829, 2023.
- [34] Sosuke Kobayashi, Eiichi Matsumoto, and Vincent Sitzmann. Decomposing nerf for editing via feature field distillation. In *Proceedings of the Advances in Neural Information Processing Systems*, volume 35, pages 23311–23330, 2022.
- [35] Xingxing Zuo, Pouya Samangouei, Yunwen Zhou, Yan Di, and Mingyang Li. Fmgs: Foundation model embedded 3d gaussian splatting for holistic 3d scene understanding. *arXiv preprint arXiv:2401.01970*, 2024.
- [36] Jin-Chuan Shi, Miao Wang, Hao-Bin Duan, and Shao-Hua Guan. Language embedded 3d gaussians for open-vocabulary scene understanding. *arXiv preprint arXiv:2311.18482*, 2023.
- [37] Minghan Qin, Wanhua Li, Jiawei Zhou, Haoqian Wang, and Hanspeter Pfister. Langsplat: 3d language gaussian splatting. In *Proceedings of the IEEE/CVF Conference on Computer Vision and Pattern Recognition*, 2024.
- [38] Georgios Kopanas, Julien Philip, Thomas Leimkühler, and George Drettakis. Point-based neural rendering with per-view optimization. In *Computer Graphics Forum*, volume 40, pages 29–43. Wiley Online Library, 2021.
- [39] Shimon Ullman. The interpretation of structure from motion. *Proceedings of the Royal Society of London. Series B. Biological Sciences*, 203(1153):405–426, 1979.
- [40] Johannes L Schonberger and Jan-Michael Frahm. Structure-from-motion revisited. In *Proceedings of the IEEE conference on computer vision and pattern recognition*, pages 4104–4113, 2016.
- [41] Matthias Zwicker, Hanspeter Pfister, Jeroen Van Baar, and Markus Gross. Ewa volume splatting. In *Proceedings Visualization, 2001. VIS'01.*, pages 29–538. IEEE, 2001.
- [42] Ho Kei Cheng, Seoung Wug Oh, Brian Price, Alexander Schwing, and Joon-Young Lee. Tracking anything with decoupled video segmentation. In *Proceedings of the IEEE/CVF International Conference on Computer Vision*, pages 1316–1326, 2023.
- [43] Julian Straub, Thomas Whelan, Lingni Ma, Yufan Chen, Erik Wijmans, Simon Green, Jakob J Engel, Raul Mur-Artal, Carl Ren, Shobhit Verma, et al. The replica dataset: A digital replica of indoor spaces. *arXiv preprint arXiv:1906.05797*, 2019.
- [44] Angela Dai, Angel X Chang, Manolis Savva, Maciej Halber, Thomas Funkhouser, and Matthias Nießner. Scannet: Richly-annotated 3d reconstructions of indoor scenes. In *Proceedings of the IEEE conference on computer vision and pattern recognition*, pages 5828–5839, 2017.
- [45] Angela Dai, Matthias Nießner, Michael Zollhöfer, Shahram Izadi, and Christian Theobalt. Bundlefusion: Real-time globally consistent 3d reconstruction using on-the-fly surface reintegration. *ACM Transactions on Graphics*, 36(4):1, 2017.
- [46] Richard Zhang, Phillip Isola, Alexei A Efros, Eli Shechtman, and Oliver Wang. The unreasonable effectiveness of deep features as a perceptual metric. In *Proceedings of the IEEE conference on computer vision and pattern recognition*, pages 586–595, 2018.